



Cite this: *Chem. Commun.*, 2019, 55, 13374

Received 3rd August 2019,  
Accepted 11th October 2019

DOI: 10.1039/c9cc06043j

rsc.li/chemcomm

# A glucose-depleting silica nanosystem for increasing reactive oxygen species and scavenging glutathione in cancer therapy†

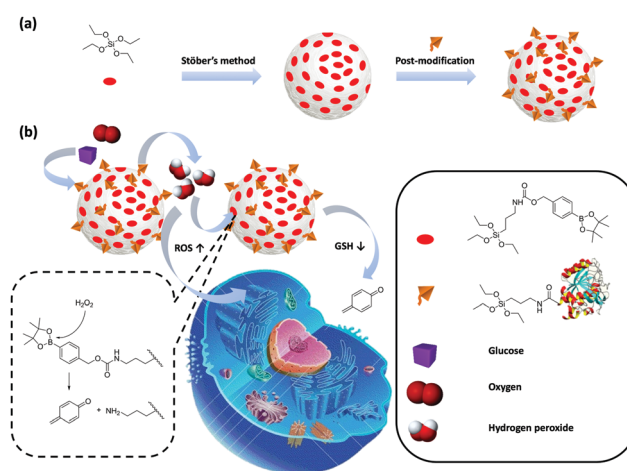
Wee Kong Ong, Deblin Jana and Yanli Zhao \*

**Cancer cells adapt to cellular oxidative stress by increasing glutathione (GSH). An organically modified silica nanosystem (ORMOSIL@GOx) was fabricated to achieve a lethal level of oxidative stress in cancer cells by depleting intracellular GSH while increasing reactive oxygen species.**

The use of reactive oxygen species (ROS) for cancer therapy is controversial because it has been reported to promote cancer growth.<sup>1,2</sup> On the other hand, more comprehensive studies have proven that ROS can kill cancer cells by elevating oxidative stress to a toxic level.<sup>3,4</sup> This process can be achieved by increasing ROS and reducing antioxidants.<sup>5</sup> To date, this strategy usually revolves around the use of polymers and prodrugs.<sup>6–8</sup> Nevertheless, challenges such as synthetic complexity, drug leakage, and insufficient targeting hindered the progression toward clinical translation.<sup>9</sup> Moreover, most systems require external energy sources or drug cargos, further limiting their effectiveness.<sup>10–12</sup>

Silica nanomaterials are endowed with simple synthesis, superior stability, biocompatibility, and scalability, and accepted as “generally recognized as safe” by the US FDA.<sup>13,14</sup> The abundance of silanol groups on the surface also facilitates post-modifications for additional functions.<sup>15</sup> Protocols based on the Stöber method enable precise control of the nanoparticle size.<sup>16</sup> This control allows for enhanced permeation and retention (EPR) effect for passive targeting.<sup>17</sup> These properties would compensate for the challenges mentioned above. However, the use of organically modified silica (ORMOSIL) nanosystems for simultaneous glutathione (GSH) depletion and ROS generation has not been well studied.<sup>18</sup>

Herein, we report the fabrication of an organically-modified silica nanosystem (ORMOSIL@GOx) in two steps (Scheme 1).<sup>19</sup> First, a bornate ester-protected quinone methide silane ligand was co-condensed with tetraethyl orthosilicate (TEOS) in a templated sol–gel methodology, followed by a post-modification with (3-aminopropyl)triethoxysilane-conjugated glucose oxidase



**Scheme 1** Schematic illustration of (a) fabrication of ORMOSIL and ORMOSIL@GOx and (b) therapeutic mechanism via ROS generation, ROS-triggered QM release, and glucose depletion. Cell image was taken using Medira software (2012) on Wikimedia Commons.

(APTES-GOx). Each component introduced is critical in treating cancer. The bornate ester-protected quinone methide silane is the first silica precursor. It is cleaved to release *p*-quinomethane (QM) in response to hydrogen peroxide.<sup>20</sup> The resulting QM would in turn react with GSH to form a GSH-QM adduct. This process not only depletes the level of GSH, but also recovers the amine group of APTES. Although it is well known that cancer cells have a higher level of hydrogen peroxide, it is insufficient to release QM rapidly.<sup>21</sup> As such, it is essential to include a component that can generate hydrogen peroxide. GOx is an enzyme that converts intracellular glucose in cancer cells into hydrogen peroxide.<sup>22,23</sup> The carboxylic group on the enzyme can react with APTES in the presence of *N*-hydroxysuccinimide to form the second silica precursor, APTES-GOx (Scheme S1, ESI†).<sup>24</sup> After the incorporation onto the silica nanoparticle surface, APTES-GOx not only produces additional hydrogen peroxide, but also starves cancer cells in terms of decreasing their glucose supply.<sup>25</sup> Equally importantly, hydrogen peroxide from APTES-GOx

Division of Chemistry and Biological Chemistry, School of Physical and Mathematical Sciences, Nanyang Technological University, 21 Nanyang Link, Singapore 637371, Singapore. E-mail: zhaoyanli@ntu.edu.sg

† Electronic supplementary information (ESI) available: Synthesis and characterization details. See DOI: 10.1039/c9cc06043j

serves as a source of ROS. This increase in ROS and the decrease in GSH increase the oxidative stress level in cancer cells above the apoptosis threshold.<sup>26</sup> One may argue that it is sufficient to simply further increase ROS to kill cancer cells. But, cancer cells can adapt by generating GSH to counteract ROS.<sup>27</sup> Hence, the released QM is important in weakening the antioxidant ability of cancer cells.<sup>28</sup> Thus, in this paper, we present a proof-of-concept of using the responsive ORMOSIL@GOx for anticancer application. This functional nanosystem provides simultaneous consumption of glucose supply, increase of intracellular oxidative stress, and suppression of antioxidants.

The bornate ester-protected quinone methide silane ligand was prepared in a two-step synthetic route by first reacting 4-(hydroxymethyl)phenylboronic acid with carbonyldiimidazole, followed by a conjugation with APTES in dimethylamino-pyridine. The chemical structures of successive compounds were well characterized by <sup>1</sup>H and <sup>13</sup>C NMR spectroscopy (Fig. S1 and S2, ESI†). Before utilizing the ligand for the templated sol-gel synthesis, we investigated whether the ligand can be specifically cleaved by hydrogen peroxide to release QM. <sup>1</sup>H NMR analysis was employed to study the release of QM in deionized water and 1 mM H<sub>2</sub>O<sub>2</sub> aqueous solution, respectively. Five new NMR peaks corresponding to 4-hydroxybenzyl alcohol were identified only in the H<sub>2</sub>O<sub>2</sub> aqueous solution, including a phenolic proton at 9.2 ppm, two aromatic doublets at 6.8 and 7 ppm, hydroxyl peak at 5.9 ppm and aliphatic singlet at 4.3 ppm (Fig. 1a). 4-Hydroxybenzyl alcohol was the hydrolyzed product of QM, which means that the preparation of this silane ligand was successful. The silane ligand is dormant in

deionized water, but would react with the hydrogen peroxide provided to generate QM.

Encouraged by the above results, the silane ligand was added jointly with TEOS to form the primary organically modified silica nanoparticles (ORMOSIL).<sup>29</sup> ORMOSIL was later modified with APTES-GOx to form ORMOSIL@GOx. Bare silica nanoparticles (SiNP) were also fabricated as the unmodified control to ORMOSIL. The fabrication of the respective nanoparticles was characterized by powder X-ray diffraction (XRD), Brunauer–Emmett–Teller (BET) surface area, scanning electron microscopy (SEM), transmission electron microscopy (TEM), X-ray photoelectron spectroscopy (XPS), dynamic light scattering (DLS) and zeta potential. The XRD analysis reveals a broad peak between 15 and 35° for all nanosystems (Fig. S3, ESI†), matching well with the reported peaks of amorphous silica.<sup>30</sup> The BET isotherm patterns indicate the low porous properties of the as-synthesized ORMOSIL and ORMOSIL@GOx (Fig. S4, ESI†). The TEM images show that ORMOSIL and ORMOSIL@GOx have spherical structures of 45 ± 3 and 75 ± 2 nm in diameter, respectively (Fig. S5 and S6, ESI†). Indeed, the SEM image of ORMOSIL@GOx also shows a spherical morphology with a diameter of around 100 nm (Fig. S7, ESI†). The zoomed-in image validates the low porous nature of ORMOSIL and ORMOSIL@GOx (Fig. S8, ESI†). The lack of mesopores would hinder the access of hydrogen peroxide to the silane ligand and result in sustained release of QM. The DLS results present larger hydrodynamic sizes of 155 ± 25, 108 ± 10 and 150 ± 10 nm for SiNP, ORMOSIL and ORMOSIL@GOx, respectively (Fig. S9, ESI†). Obvious zeta potential fluctuation after each reaction step demonstrates the integration of the silane ligand from −21.7 mV in SiNP to +26 mV in ORMOSIL, effective removal of the CTAB template in ORMOSIL from +26 mV to +7.79 mV, and the incorporation of APTES-GOx from +7.79 mV to 18.2 mV (Fig. S10, ESI†). XPS comparison between SiNP and ORMOSIL reveals an additional boron 1s peak in the latter, further confirming the successful incorporation of the silane ligand (Fig. S11, ESI†). A new UV-vis absorbance peak corresponding to 4-(hydroxymethyl)phenylboronic acid pinacol ester (4-HPBA) appears upon incorporation of the silane ligand into ORMOSIL (Fig. S12, ESI†). 4-HPBA has an intense absorbance peak at 225 nm because of its aromaticity. However, this peak drastically decreases after covalent conjugation with APTES-GOx, attributing to the effective surface loading of APTES-GOx on ORMOSIL.

To further confirm the attachment of APTES-GOx on the ORMOSIL surface, fluorescence labeling and thermogravimetric analysis (TGA) were conducted. In the former study, GOx was initially labeled with fluorescein isothiocyanate (FITC) before the conjugation with APTES.<sup>25</sup> According to a given formula, the number of labeled FITC per GOx was 4.2 units (Fig. S13, ESI†). The FITC-labeled GOx was further reacted with APTES and then ORMOSIL to form FITC-labeled ORMOSIL@GOx. By matching the fluorescence of FITC-labeled ORMOSIL@GOx to the calibration curve, the GOx loading was determined to be 9.3 wt% (Fig. S14, ESI†). Michaelis–Menten steady-state kinetics was used to determine the catalytic performance of ORMOSIL@GOx toward glucose conversion to hydrogen peroxide (Fig. 1c and d).

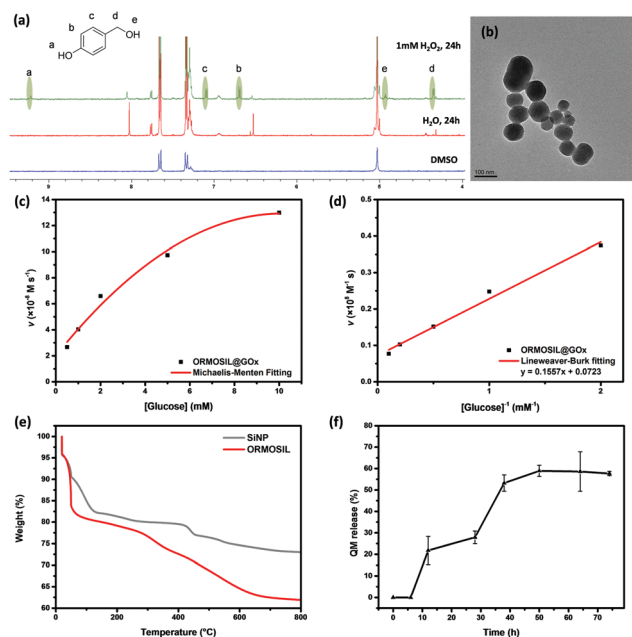


**Fig. 1** (a) QM release in the presence and absence of H<sub>2</sub>O<sub>2</sub> recorded by <sup>1</sup>H NMR spectra. (b) TEM image of ORMOSIL@GOx. Scale bar: 100 nm. (c) Michaelis–Menten kinetics of ORMOSIL@GOx. (d) Lineweaver–Burk plotting of ORMOSIL@GOx. (e) TGA comparison of SiNP and ORMOSIL for the determination of the silane ligand content. (f) Release of QM from ORMOSIL@GOx (10 mg mL<sup>-1</sup>) in 5 mg mL<sup>-1</sup> glucose. Mean ± s.d., n = 3.

The Michaelis–Menten constant ( $K_m$ ) and maximum velocity ( $V_{max}$ ) of ORMOSIL@GOx were calculated to be 44.7 mM and  $12.8 \times 10^{-8} \text{ M s}^{-1}$ , respectively (Table S1, ESI†). The  $K_m$  value is comparable to the commercially available GOx between 33 and 110 mM, meaning that for 44.7 mM of glucose about half of the maximum catalytic activity could be achieved.

It is also important to characterize the QM component content of ORMOSIL@GOx. TGA comparison between SiNP and ORMOSIL shows a weight difference of 11%, corresponding to the additional weight from the silane ligand (Fig. 1e). From this result, the loading efficiency of the silane ligand in ORMOSIL was calculated to be 59% (Fig. S15, ESI†). Since each silane ligand holds a unit of QM, the total QM content could similarly be calculated to be  $0.229 \text{ mmol g}^{-1}$  of ORMOSIL. The cumulative QM release profile indicates that the release of QM starts after the 7 h mark (Fig. 1f). This observation is attributed to the low porous nature of ORMOSIL@GOx, which restricts the access of hydrogen peroxide to the silane ligand. The release occurs rapidly until its plateau after 50 h, giving approximately 60% total release. QM released from the bornate ester-protected QM silane ligand is very reactive, and it would eventually be hydrolyzed to produce 4-hydroxybenzyl alcohol in aqueous medium. In a GSH-rich medium such as the lysosome of cancer cells, 4-hydroxybenzyl alcohol could produce the GSH-adduct *via* thiol substitution at the allylic alcohol (Scheme 1). Liquid chromatography-mass spectrometry analysis of ORMOSIL@GOx incubated in 1 mM glucose and 1 mM GSH over 24 h reveals a distinct peak at 412 *m/z*, attributing to the GSH-adduct (Fig. S16, ESI†). This is direct evidence of its GSH scavenging ability.

*In vitro* studies were conducted to investigate the cytotoxicity and cellular effectiveness of the nanosystems. The half maximal inhibitory concentration ( $IC_{50}$ ) of SiNP is  $2140 \mu\text{g mL}^{-1}$ , while the  $IC_{50}$  of ORMOSIL is  $753 \mu\text{g mL}^{-1}$  (Fig. S19, ESI†). This decrease is attributed to the incorporation of the silane ligand that increases the hydrophobicity of the nanosystem. At the same time, the released QM could disrupt the ROS homeostasis in cancer cells. Nonetheless, a high concentration of  $200 \mu\text{g mL}^{-1}$  only yielded 29% killing efficiency, indicating that QM alone is inadequate for effective cancer therapy (Fig. 2a and b). On the other hand, the cellular results reflect the exceptionally low cytotoxicity of ORMOSIL relative to the control groups. Since GOx serves as the main source of hydrogen peroxide and is subsequently conjugated to the surface of ORMOSIL, it is important to determine the cytotoxicity of GOx so that a healthy amount of the GOx equivalent is used for cellular studies. The GOx cytotoxicity in the presence of  $1 \text{ mg mL}^{-1}$  glucose was concentration dependent. The  $IC_{50}$  of GOx in MDA-MB-231 breast cancer cells was determined to be  $41 \text{ mU mL}^{-1}$  (Fig. S20, ESI†). 3-(4,5-Dimethylthiazol-2-yl)-2,5-diphenyltetrazolium bromide (MTT) assay was carried out using an equivalent GOx concentration of  $10 \text{ mU mL}^{-1}$ . At this range of GOx, both GOx and ORMOSIL showed high cell viability of more than 75%. Interestingly, the therapeutic efficiency greatly increased when both GOx and ORMOSIL were integrated together as ORMOSIL@GOx. The  $IC_{50}$  of ORMOSIL@GOx in MDA-MB-231 breast cancer cells was determined to be  $0.576 \mu\text{g mL}^{-1}$  or  $5.4 \text{ mU mL}^{-1}$  GOx

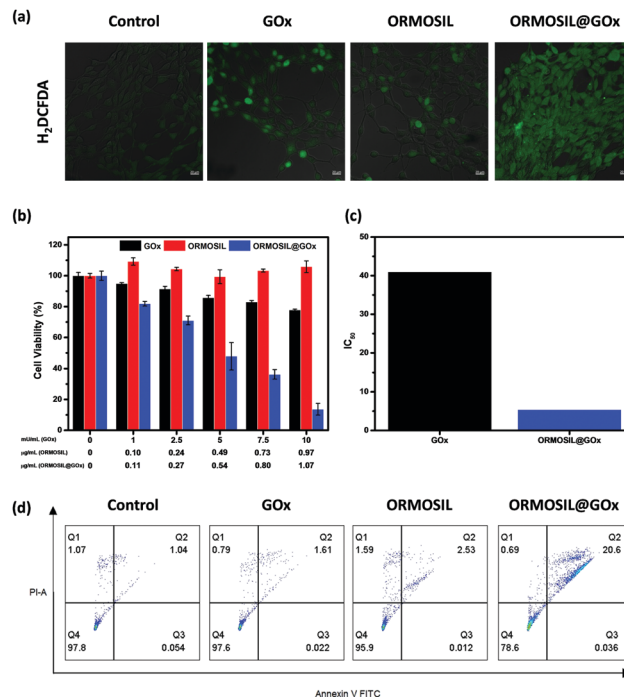
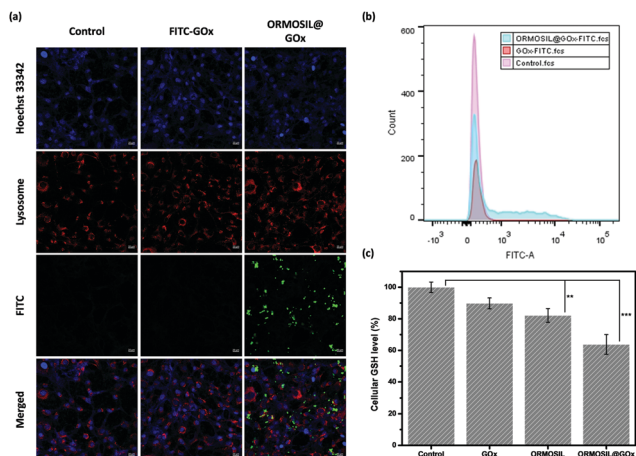


Fig. 2 *In vitro* cytotoxicity and catalytic performance. (a) Confocal images of MDA-MB-231 cells after co-incubation with PBS, GOx, ORMOSIL and ORMOSIL@GOx in  $1 \text{ mg mL}^{-1}$  glucose Dulbecco's modified Eagle medium for 4 h and subsequently stained with the ROS fluorescent probe DCFH-DA. Scale bar:  $20 \mu\text{m}$ . (b) *In vitro* cytotoxic profile of GOx, ORMOSIL and ORMOSIL@GOx at varying GOx concentrations. (c)  $IC_{50}$  comparison between free GOx and ORMOSIL@GOx. (d) Live/dead cell apoptotic assay of control, GOx, ORMOSIL, and ORMOSIL@GOx after 24 h incubation with  $10 \text{ mU mL}^{-1}$  GOx equivalents.

equivalent. This is 7.6 and 1307 times better than that of free GOx and ORMOSIL in terms of anticancer efficiency, respectively (Fig. 2c). The released QM makes antioxidant GSH to reach a sufficiently low concentration in order to enhance the cancer cell killing effect of ROS. Thus, simultaneous depletion of glucose nutrient and continued generation of hydrogen peroxide exert immense stress on cancer cells. The therapeutic outcome was again confirmed by flow cytometry analysis at a GOx concentration of  $10 \text{ mU mL}^{-1}$ . 20.6% of ORMOSIL@GOx treated cancer cells reached the late apoptotic stage compared to 1.61% and 2.53% in the case of GOx and ORMOSIL, respectively (Fig. 2d). These experimental results highlight the synergy between ORMOSIL and GOx in ORMOSIL@GOx for greatly inhibiting the cancer cell growth.

Taking the reference to Scheme S2 (ESI†), ORMOSIL@GOx initially catalyzes  $\beta$ -D-glucose into  $\beta$ -D-glucono-1,5-lactone and hydrogen peroxide. The produced hydrogen peroxide would raise the level of ROS in cancer cells. The subsequent QM release impedes the decrease of ROS scavenged by GSH. Thus, the overall oxidative stress and ROS level would be substantially higher than under normal conditions. In order to confirm that an ROS-mediated therapy occurs, an ROS fluorescent probe 2',7'-dichlorofluorescein diacetate (DCFH-DA) was used. MDA-MB-231 cells showed the highest level of green fluorescence after incubation with ORMOSIL@GOx ( $7.5 \text{ mU mL}^{-1}$  GOx equivalent)



**Fig. 3** (a) Confocal images of MDA-MB-231 cells incubated with FITC-labeled GOx and ORMOSIL@GOx after 2 h. Cell nuclei were stained by H33342. Scale bar: 20  $\mu\text{m}$ . (b) Flow cytometry profiles of MDA-MB-231 cells incubated with FITC-labeled GOx and ORMOSIL@GOx after 2 h. (c) Cellular GSH level in MDA-MB-231 cells after the incubation with PBS, GOx, ORMOSIL and ORMOSIL@GOx at an equivalent GOx concentration of 10  $\text{mU mL}^{-1}$  in the presence of 1  $\text{mg mL}^{-1}$  glucose for 24 h. Mean  $\pm$  s.d.,  $n = 3$ . \*\* $p < 0.05$ , \*\*\* $p < 0.005$  ( $t$ -test).

over 12 h (Fig. 2a). As expected, GOx and ORMOSIL exhibited stronger fluorescence than the control, but still beneath ORMOSIL@GOx. The observations indicate that, while GOx could produce a certain amount of ROS and ORMOSIL promotes a smaller amount of additional ROS, the integration of them in ORMOSIL@GOx performs perfectly to kill cancer cells by increasing ROS beyond the apoptotic level.

FITC-labeled ORMOSIL@GOx and GOx were separately incubated with MDA-MB-231 cells over 2 h to evaluate their cellular uptake (Fig. 3a and b). Fluorescence analysis by flow cytometry indicates that GOx cannot be endocytosed into cancer cells. However, obvious fluorescence detected from the ORMOSIL@GOx group means that it could be accumulated in the cells effectively, probably through a nanoparticle-based endocytosis pathway.<sup>31</sup> This observation also validates that the therapeutic effect of free GOx is limited and cannot directly treat cancer cells on its own. The results from laser confocal scanning microscopy (Fig. 3a) are agreeable to the flow cytometry analysis. ORMOSIL@GOx was observable within the lysosome regions of cancer cells, whereas no fluorescence was seen in the case of GOx.

As discussed above, QM generated by ORMOSIL@GOx could reduce the level of GSH antioxidant in cancer cells. The intracellular GSH was investigated at a concentration of 5  $\text{mU mL}^{-1}$  by flow cytometry, where the fluorescence intensity correlates with the GSH level (Fig. 3c). The fluorescence decreased to 90%, 82% and 64% within 24 h when cells were incubated with GOx, ORMOSIL and ORMOSIL@GOx, respectively, indicating better GSH-scavenging ability of ORMOSIL@GOx in cancer cells. The QM amount released from ORMOSIL@GOx was higher compared to that from ORMOSIL alone, since the latter relies solely on intrinsic intracellular hydrogen peroxide for the QM release.

In summary, a glucose-depleting silica nanosystem (ORMOSIL@GOx) has been successfully fabricated from bornate ester-protected

quinone methide silane and APTES-GOx. The nanosystem could be effectively internalized by cancer cells, converting intracellular glucose to hydrogen peroxide for enhancing the ROS level. Hydrogen peroxide in turn triggers the release of QM to scavenge GSH to achieve synergistic anticancer treatment. Importantly, *in vitro* experiments have well demonstrated this cancer treatment strategy provided by ORMOSIL@GOx. Furthermore, this nanosystem does not rely on any external input or drugs, which offers an easy platform for cancer therapy. Thus, this research is expected to pave the way for developing next generation approaches in cancer treatment.

This research was supported by the Singapore Agency for Science, Technology and Research (A\*STAR) AME IRG grant (No. A1883c0005) and the Singapore National Research Foundation Investigatorship (No. NRF-NRFI2018-03).

## Conflicts of interest

There are no conflicts to declare.

## Notes and references

- J. P. Fruehauf and F. L. Meyskens, *Clin. Cancer Res.*, 2007, **13**, 789.
- S. S. Sabharwal and P. T. Schumacker, *Nat. Rev. Cancer*, 2014, **14**, 709.
- J. Wang and J. Yi, *Cancer Biol. Ther.*, 2008, **7**, 1875.
- D. Trachootham, J. Alexandre and P. Huang, *Nat. Rev. Drug Discovery*, 2009, **8**, 579.
- M. F. Renschler, *Eur. J. Cancer*, 2004, **40**, 1934.
- J. Noh, B. Kwon, E. Han, M. Park, W. Yang, W. Cho, W. Yoo, G. Khang and D. Lee, *Nat. Commun.*, 2015, **6**, 6907.
- H. Hagen, P. Marzenell, E. Jentzsch, F. Wenz, M. R. Veldwijk and A. Mokhir, *J. Med. Chem.*, 2012, **55**, 924.
- C.-Q. Luo, Y.-X. Zhou, T.-J. Zhou, L. Xing, P.-F. Cui, M. Sun, L. Jin, N. Lu and H.-L. Jiang, *J. Controlled Release*, 2018, **274**, 56.
- S. Mura, J. Nicolas and P. Couvreur, *Nat. Mater.*, 2013, **12**, 991.
- C. Argyo, V. Weiss, C. Bräuchle and T. Bein, *Chem. Mater.*, 2014, **26**, 435.
- A. Y. Rwei, W. Wang and D. S. Kohane, *Nano Today*, 2015, **10**, 451.
- Y. Lu, Y. Yang, Z. Gu, J. Zhang, H. Song, G. Xiang and C. Yu, *Biomaterials*, 2018, **175**, 82.
- M. Vallet-Regi, A. Rámila, R. P. del Real and J. Pérez-Pariente, *Chem. Mater.*, 2001, **13**, 308.
- J. Lu, M. Liong, Z. Li, J. I. Zink and F. Tamanoi, *Small*, 2010, **6**, 1794.
- I. I. Slowing, J. L. Vivero-Escoto, C.-W. Wu and V. S. Y. Lin, *Adv. Drug Delivery Rev.*, 2008, **60**, 1278.
- S.-H. Wu, C.-Y. Mou and H.-P. Lin, *Chem. Soc. Rev.*, 2013, **42**, 3862.
- N. Poonia, V. Lather and D. Pandita, *Drug Discovery Today*, 2018, **23**, 315.
- R. Kumar, I. Roy, T. Y. Ohulchanskyy, L. A. Vathy, E. J. Bergey, M. Sajjad and P. N. Prasad, *ACS Nano*, 2010, **4**, 699.
- T. Y. Ohulchanskyy, I. Roy, L. N. Goswami, Y. Chen, E. J. Bergey, R. K. Pandey, A. R. Oseroff and P. N. Prasad, *Nano Lett.*, 2007, **7**, 2835.
- W. Yin, J. Li, W. Ke, Z. Zha and Z. Ge, *ACS Appl. Mater. Interfaces*, 2017, **9**, 29538.
- M. López-Lázaro, *Cancer Lett.*, 2007, **252**, 1.
- L.-H. Fu, C. Qi, J. Lin and P. Huang, *Chem. Soc. Rev.*, 2018, **47**, 6454.
- L.-H. Fu, C. Qi, Y.-R. Hu, J. Lin and P. Huang, *Adv. Mater.*, 2019, **31**, 1808325.
- S. Libertino, V. Aiello, A. Scandurra, M. Renis and F. Sinatra, *Sensors*, 2008, **8**, 5637.
- W. Fan, N. Lu, P. Huang, Y. Liu, Z. Yang, S. Wang, G. Yu, Y. Liu, J. Hu, Q. He, J. Qu, T. Wang and X. Chen, *Angew. Chem., Int. Ed.*, 2017, **56**, 1229.
- P. T. Schumacker, *Cancer Cell*, 2006, **10**, 175.
- R. A. Cairns, I. S. Harris and T. W. Mak, *Nat. Rev. Cancer*, 2011, **11**, 85.
- A. Glasauer and N. S. Chandel, *Biochem. Pharmacol.*, 2014, **92**, 90.
- J. G. Croissant, J. I. Zink, L. Raehm and J.-O. Durand, *Adv. Healthcare Mater.*, 2018, **7**, 1701248.
- S. Musi, N. Filipovi-Vincekovi and L. Sekovani, *Braz. J. Chem. Eng.*, 2011, **28**, 89.
- L. Kou, J. Sun, Y. Zhai and Z. He, *Asian J. Pharm. Sci.*, 2013, **8**, 1.